

Morphogenesis by coupled regulatory networks

Thimo Rohlf and Stefan Bornholdt

Interdisciplinary Center for Bioinformatics, University of Leipzig, Kreuzstraße 7b, D-04102 Leipzig, Germany

(Dated: October 27, 2018)

Based on a recently proposed non-equilibrium mechanism for spatial pattern formation [13] we study how morphogenesis can be controlled by locally coupled discrete dynamical networks, similar to gene regulation networks of cells in a developing multicellular organism. As an example we study the developmental problem of domain formation and proportion regulation in the presence of noise and cell flow. We find that networks that solve this task exhibit a hierarchical structure of information processing and are of similar complexity as developmental circuits of living cells. A further focus of this paper is a detailed study of noise-induced dynamics, which is a major ingredient of the control dynamics in the developmental network model. A master equation for domain boundary readjustments is formulated and solved for the continuum limit. Evidence for a first order phase transition in equilibrium domain size at vanishing noise is given by finite size scaling. A second order phase transition at increased cell flow is studied in a mean field approximation. Finally, we discuss potential applications.

PACS: 87.18.Hf, 05.70.Ln, 05.50.+q

I. INTRODUCTION

Understanding the molecular machinery that regulates development of multicellular organisms is among the most fascinating problems of modern science. Today, a growing experimental record about the regulatory mechanisms involved in development is accumulating, in particular in well-studied model-organisms as, e.g., *Drosophila* or *Hydra* [1, 2]. Still, the genomic details known today are not sufficient to derive dynamical models of developmental gene regulation processes in full detail. Phenomenological models of developmental processes, on the other hand, are well established today. Pioneering work in this field was done by Turing, who in his seminal paper in 1952 [3] considered a purely physico-chemical origin of biological pattern formation. His theory is based on an instability in a system of coupled reaction-diffusion equations. In this type of model, for certain parameter choices, stochastic fluctuations in the initial conditions can lead to self-organization and maintenance of spatial patterns, e.g. concentration gradients or periodic patterns. This principle has been successfully applied to biological morphogenesis in numerous applications [4, 5]. However, as current experiments make us wonder about the astonishingly high complexity of single regulating genes in development [6], they also seem to suggest that diffusion models will not be able to capture all details of developmental regulation, and point at a complex network of regulating interactions instead.

The role of information processing in gene regulatory networks during development has entered the focus of theoretical research only recently. One pioneering study was published by Jackson et al. [7] in 1986, who investigated the dynamics of spatial pattern formation in a system of locally coupled, identical dynamical networks. In this model, gene regulatory dynamics is approximated by Boolean networks with a subset of nodes communicating not only with nodes in the (intracellular) network, but

also with some nodes in the neighboring cells. Boolean networks are minimal models of information processing in network structures and have been discussed as models of gene regulation since the end of the 1960s [8, 9]. The model of Jackson et al. demonstrated the enormous pattern forming potential of local information processing, similar to *direct contact induction* [10] as known in developmental biology. More recently, Salazar-Ciudad et al. introduced a gene network model based on continuous dynamics [11, 12] and coupling their networks by direct contact induction. Interestingly, they observe a larger variety of spatial patterns than Turing-type models with diffusive morphogens, and find that patterns are less sensitive to initial conditions, with more time-independent (stationary) patterns. This matches well the intuition that networks of regulators have the potential for more general dynamical mechanisms than diffusion driven models. Let us here therefore study interacting networks in pattern formation and in particular consider information-transfer-based processes. In [13], we introduced a simple stochastic cellular automata model of spatial pattern formation based on local information transfer, that performs de novo pattern formation by generating and regulating a domain boundary. In the following we will study how this very general mechanism could emerge as a result of interacting nodes in coupled identical networks, similar to gene regulation networks in interacting cells.

The goal of this paper is twofold: First we will explore ways to map the earlier cellular automata model [13], onto dynamical networks (Boolean networks and threshold networks), motivated by the general observation of gene regulation networks in biological development (section III). Secondly, we will give a more detailed account of the basic underlying mechanism, focusing on the stochastic dynamics (section IV) and on how the model was developed using a genetic algorithm (Appendix): In section IV, the statistical mechanics of noise-induced dynamics

is studied in detail. Numerical evidence for a first order phase transition at vanishing noise rate is given. A master equation for boundary readjustments is formulated and solved in the continuum limit. Robustness against cell flow is studied numerically and in a mean field approximation. In the Appendix, the genetic algorithm applied for identification of model solutions is explained and statistical properties of different solutions are compared.

II. PROBLEM AND MODEL

Let us first motivate and define the morphogenetic problem that we will use as a test case. Then we undertake a three-step approach to find a genetic network model that solves this pattern formation problem. In the first step, we summarize the properties of the cellular automata model introduced in [13]. Cellular automata as dynamical systems discrete in time and state space are known to display a wide variety of complex patterns [14] and are capable of solving complex computational tasks, including universal computation. We searched for solutions (i.e. rule tables which solve the problem) by aid of a genetic algorithm (for details, see Appendix). Candidate solutions have to fulfill four demands: Their update dynamics has to generate a spatial pattern which 1) obeys a predefined scaling ratio $\alpha/(1-\alpha)$, 2) is independent of the initial condition chosen at random, 3) is independent of the system size (i.e. the number of cells N_C) and 4) is stationary (a fixed point). In the second step, this cellular automata rule table is “translated” into (spatially coupled) Boolean networks, using binary coding of the cellular automata states. The logical structure of the obtained network is reduced to a minimal form, and then, in step three, translated into a threshold network.

A. A test scenario: Hydra foot formation

A classical model organism for studies of position dependent gene activation is the fresh water polyp *Hydra*, which has three distinct body regions - a head with mouth and tentacles, a body column and a foot region. The positions of these regions are accurately regulated along the body axis.

The problem we shall focus on is sketched schematically in Fig. 1 for the example of the “foot” genes *Pedibin* and *CN-NK2* [15]. *CN-NK2* is active only in the lowest foot region, the expression domain of *Pedibin* extends a bit more towards the rump region, where it is turned off at some point, i.e. the domain shows a sharp boundary. The relative position of the boundary is almost independent of the animal’s size, i.e. the ratio $\alpha/(1-\alpha)$ (as denoted in Fig. 1) is almost invariant under changes of body size. As the *Pedibin/CN-NK2* system presumably plays an important role in determining the foot region, this invariance appears to be an essential prerequisite for maintaining the correct body proportions (proportion

regulation) and to establish the head-foot polarity. Such regulation of position information is a quite general problem in biological development [16]. An interesting problem is how the specific properties of this regulation can be achieved by a small network of regulatory genes and if so, whether local communication between the cells (networks) is sufficient. This basic question is the central motivation for the present study. In particular, we consider the simplified problem of regulating one domain as, for example, the foot region versus the rest of the body. We consider this as a one dimensional problem as first approximation to the well-defined head-foot-axis in *Hydra*.

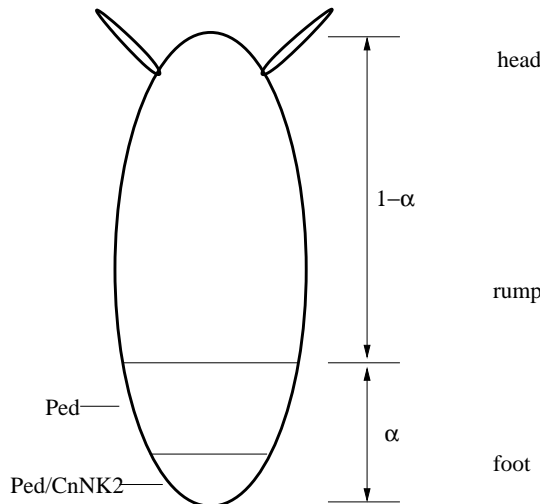


FIG. 1: Gene expression domains in *Hydra*, here for the example of the “foot” genes *Pedibin* (*Ped*) and *Cn-NK2*. The *Pedibin* domain shows a quite sharp boundary towards the body region of the animal. The relative position of the boundary, given by the ratio $\alpha/(1-\alpha)$, is independent of the absolute size of the animal (proportion regulation).

Developmental processes exhibit an astonishing robustness. This often includes the ability of *de novo* pattern formation, e.g., to regenerate a *Hydra* even after complete dissociation of the cell ensemble in a centrifuge [17]. Further, they are robust in the face of a steady cell flux: *Hydra* cells constantly move from the central body region along the body axis towards the top and bottom, where they differentiate into the respective cell types according to their position on the head-foot axis. The global pattern of gene activity is maintained in this dynamic environment. Let us take these observations as a starting point for a detailed study how the interplay of noise-induced regulatory dynamics and cell flow may stabilize a developmental system.

B. One dimensional cellular automata: Definitions

To define a model system that performs the pattern formation task of domain self-organization [13], consider

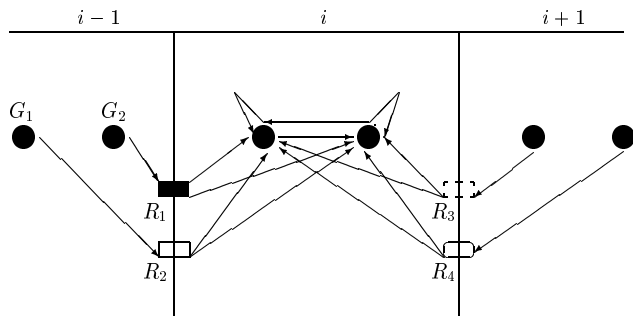


FIG. 2: Diagram showing the interaction structure of the minimal network needed to solve the asymmetric expression task. For the sake of clarity, intracellular interactions between the two genes G_1 and G_2 are shown only for cell i , and likewise outgoing intercellular signals from the two genes to the neighbor cells $i-1$ and $i+1$ were left out. The transcription factors produced by gene G_1 and G_2 in cell $i-1$ couple to the receptor systems R_1 and R_2 , respectively, whereas in cell $i+1$ the transcription factors produced by these genes couple to the receptor systems R_3 and R_4 (biased signaling). In cell i , the receptors release factors which regulate the activity of G_1 and G_2 .

a one-dimensional cellular automaton with parallel update [14]. N_C cells are arranged on a one-dimensional lattice, and each cell is labeled uniquely with an index $i \in \{0, 1, \dots, N_C - 1\}$. Each cell can take n possible states $\sigma_i \in \{0, 1, \dots, n\}$. The state $\sigma_i(t)$ of cell i is a function of its own state $\sigma_i(t-1)$ and of its neighbor's states $\sigma_{i-1}(t-1)$ and $\sigma_{i+1}(t-1)$ at time $t-1$, i.e.

$$\sigma_i(t) = f[\sigma_{i-1}(t-1), \sigma_i(t-1), \sigma_{i+1}(t-1)] \quad (1)$$

with $f : \{0, 1, \dots, n\}^3 \mapsto \{0, 1, \dots, n\}$ (a cellular automaton with *neighborhood 3*). At the system boundaries, for simplicity we choose a discrete analogue of zero flux boundary conditions, i.e. we set $\sigma_{-1} = \sigma_{N_C+1} = \text{const.} = 0$. Other choices, e.g. asymmetric boundaries with cell update depending only on the inner neighbor cell, lead to similar results. The state evolution of course strongly depends on the choice of f : for a three-state cellular automaton ($n = 3$), there are $3^{27} \approx 7.626 \cdot 10^{12}$ possible update rules, each of which has a unique set of dynamical attractors. As we will show in the results section, $n = 3$ is the minimal number of states necessary to solve the pattern formation problem formulated above.

Now we can formulate the problem we intend to solve as follows: Find a set \mathcal{F} of functions (update rules) which, given a random initial vector $\vec{\sigma} = (\sigma_0, \dots, \sigma_{N_C-1})$, within T update steps evolves the system's dynamics to a fixed point attractor with the property:

$$\vec{\sigma}^* := \begin{cases} \sigma_i = 2 & \text{if } i < [\alpha \cdot N_C] \\ \sigma_i \neq 2 & \text{if } i \geq [\alpha \cdot N_C] \end{cases} \quad (2)$$

where $[\cdot]$ is the Gauss bracket. The scaling parameter α may take any value $0 < \alpha < 1$. For simplicity, it is fixed here to $\alpha = 0.3$. Notice that α does not depend

on N_C , i.e. we are looking for a set of solutions where the ratio of the domain sizes $r := \alpha/(1-\alpha)$ is *invariant under changes of the system size*. This clearly is a non-trivial task when only local information transfer is allowed. The ratio r is a *global property* of the system, which has to emerge from purely local (next neighbor) interactions between the cell's states.

C. Translation into spatially coupled Boolean networks

One can now take a step further towards biological systems, by transferring the dynamics we found for a cellular automata chain onto cells in a line that communicate with each other, similar to biological cells. Identifying states with cell types and assuming that the model cells have a network of regulators inside, each of them capable to reproduce the rules of a cellular automaton, we obtain a model mimicking basic properties of a biological genetic network in development.

Cellular automata rule tables can easily be translated into logical (Boolean) networks, e.g., for $n = 3$, two internal nodes can be used for binary coding of the cell states. One then has

$$(\sigma_1^i(t), \sigma_2^i(t)) = f_1(\sigma_{1,2}^{i-1}(t-1), \sigma_{1,2}^i(t-1), \sigma_{1,2}^{i+1}(t-1)) \quad (3)$$

with $f_1 : \{0, 1\}^6 \mapsto \{0, 1\}^2$. The so obtained rule tables are, by application of Boolean logic, transformed into a minimized *conjunctive normal form*, which only makes use of the three logical operators NOT, AND and OR with a minimal number of AND operations. This is a rather realistic assumption for gene regulatory networks, as the AND operation is more difficult to realize on the basis of interactions between transcription factors. Other logical functions as, e.g., XOR, are even harder to realize biochemically [18]. The structure of the constructed network and its biological interpretation is shown in Fig. 2. Note that the up-down symmetry of the body axis is broken locally by a spatially asymmetric receptor distribution [19].

D. Translation into spatially coupled threshold networks

Perhaps the simplest model for transcriptional regulation networks are threshold networks, a subset of Boolean networks, where logical functions are modeled by weighted sums of the nodes' input states plus a threshold h [20, 21]. They have proven to be valuable tools to address questions associated to the dynamics and evolution of gene regulatory networks [22, 23, 24, 25, 26].

Any Boolean network which has been reduced to its minimized form (here, the conjunctive normal form), can be coded as a dynamical threshold network, with minimally three hierarchies of information processing ("input

layer”: signals from the neighbor cells at time $t - 1$, “hidden layer”: logical processing of the signals, “output layer”: states of the two “pattern genes” in cell i at time t). The genes’ states now may take values $\sigma_i = \pm 1$, and likewise for the interaction weights one has $c_{ij}^l = \pm 1$ for activating and inhibiting regulation, respectively, and $c_{ij}^l = 0$ if gene i does not receive an input from gene j in cell l . The dynamics then is defined as

$$\sigma_j^i(t) = \text{sign}(f_j(t-1)) \quad (4)$$

with

$$f_j(t) = \sum_{k=1}^2 \sum_{l=i-1}^{i+1} c_{kj}^l \sigma_k^l + h_j \quad (5)$$

for the “hidden” genes, where $\sigma_k^l, k \in \{1, 2\}$ is the state of the k th *output* gene in cell l (there are no couplings between the genes in the “hidden” layer). The threshold h_j is given by

$$h_j = \sum_{k=1}^2 \sum_{l=i-1}^{i+1} |c_{kj}^l| - 2, \quad (6)$$

which implements a logical OR operation. For the “output” (pattern forming) genes, one simply has

$$f_k(t) = \sum_{l=1}^{k_{in}^k} \sigma_l - k_{in}^k, \quad (7)$$

i.e. the weights are all set to one, and the (negative) threshold equals the number of inputs k_{in}^k that gene k receives from the “hidden” genes (logical AND).

III. RESULTS FOR DETERMINISTIC DYNAMICS

A. Cellular Automata Model

The first major outcome of the cellular automata model is that a number of $n = 3$ different states is necessary and sufficient for this class of systems to solve the given pattern formation task. The update table of the fittest solution found during optimization runs, which solves the problem independent of system size for about 98 percent of (randomly chosen) initial conditions (i.e. has fitness $\Phi = 0.98$), is shown in Table I. Fig. 3 shows the typical update dynamics of this solution. The finite size scaling of the self-organized relative domain size α as a function of the the number of cells N_C is shown in Fig. 4. In the limit of large system sizes, α converges towards

$$\alpha_\infty = 0.281 \pm 0.001. \quad (8)$$

The variance of α vanishes with a power of N_C , i.e. the relative size of fluctuations induced by different initial

conditions becomes arbitrarily small with increasing system size. Hence, the pattern self-organization in this system exhibits considerable robustness against fluctuations in the initial conditions. The main mechanism leading to stabilization at $\alpha_\infty = 0.281$ is a modulation of the traveling velocity of the right phase boundary in Fig. 2 such that the boundary on average moves slightly more than one cell to the left per update step, whereas the left boundary moves one cell to the right exactly every third update step. the modulation of the right boundary can be seen as the result of interacting phase boundaries reminiscent of particle interactions. This picture of “particle computation” is a useful concept also in various other contexts [27].

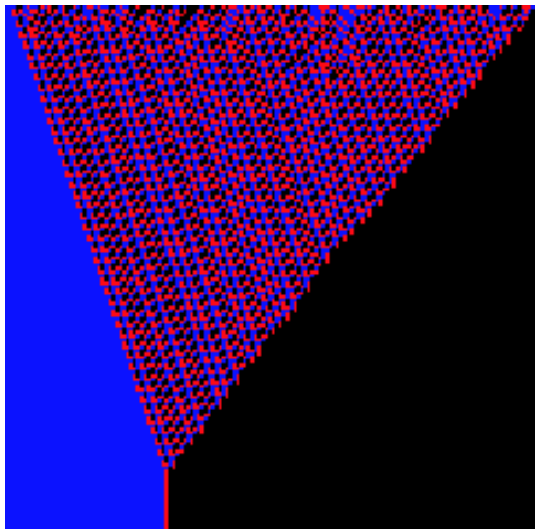


FIG. 3: A typical dynamical run for the Automata as defined in Table I, here for a system of size $N_C = 250$ cells (deterministic dynamics, no noise), starting from a random initial configuration. Time is running on the y -axis from top to bottom. Cells with state $\sigma_i = 0$ are depicted in black color, cells with $\sigma_i = 1$ in red and cells with $\sigma_i = 2$ in blue.

B. Interaction topology of the minimal network

In this section let us translate the rule table found in the previous section into a (gene) regulatory network. We will see that this network has biologically realistic properties regarding the number of genes necessary for information processing and the complexity of interaction structure, making it well conceivable that similar “developmental modules” exist in biological systems.

1. Boolean representation

The rule table of Table 1 first is translated into binary coding, i.e $0 \rightarrow 00$, $1 \rightarrow 01$ and $2 \rightarrow 10$, this corresponds to two “genes” G_1 and G_2 one of which (G_1)

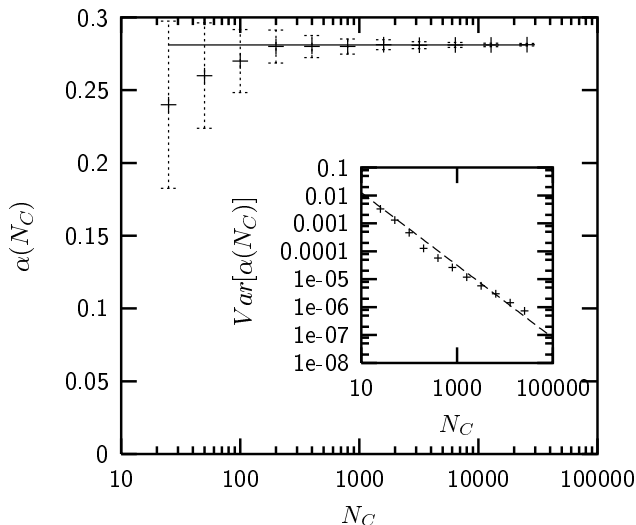


FIG. 4: Finite size scaling of the self-organized relative domain size α as a function of the total number of cells N_C . In the limit of large system sizes, α converges towards a fixed value $\alpha_\infty = 0.281 \pm 0.001$ (as denoted by the straight line fit). The inset shows the finite size scaling of the variance $\text{Var}[\alpha(N_C)]$; the straight line in this log-log plot has slope -1.3 and indicates that fluctuations vanish with a power of the system size.

index	σ_{i-1}	σ_i	σ_{i+1}	σ_i	index	σ_{i-1}	σ_i	σ_{i+1}	σ_i
0	0	0	0	0	14	1	1	2	2
1	0	0	1	2	15	1	2	0	0
2	0	0	2	1	16	1	2	1	0
3	0	1	0	0	17	1	2	2	1
4	0	1	1	2	18	2	0	0	0
5	0	1	2	2	19	2	0	1	0
6	0	2	0	1	20	2	0	2	0
7	0	2	1	2	21	2	1	0	1
8	0	2	2	2	22	2	1	1	2
9	1	0	0	0	23	2	1	2	2
10	1	0	1	1	24	2	2	0	1
11	1	0	2	1	25	2	2	1	2
12	1	1	0	0	26	2	2	2	2
13	1	1	1	1					

TABLE I: Rule table of most successful best cellular automata solution found during genetic algorithm search. In the left column, the rule table index is shown, running from 0 to 26, in the middle column the three input states at time t are shown, the right column shows the corresponding output states at time $t+1$.

is active only in a domain at the left side of the cell chain. The so obtained Boolean update table is reduced to its minimized conjunctive normal form, using a Quine-McCluskey algorithm [28]. For the construction of the network topology we use the conjunctive normal form, as it is a somewhat biologically plausible solution with a minimal number of logical AND operations. In principle, other network topologies, e.g. with more levels of hierarchy, are possible and biologically plausible, however, they

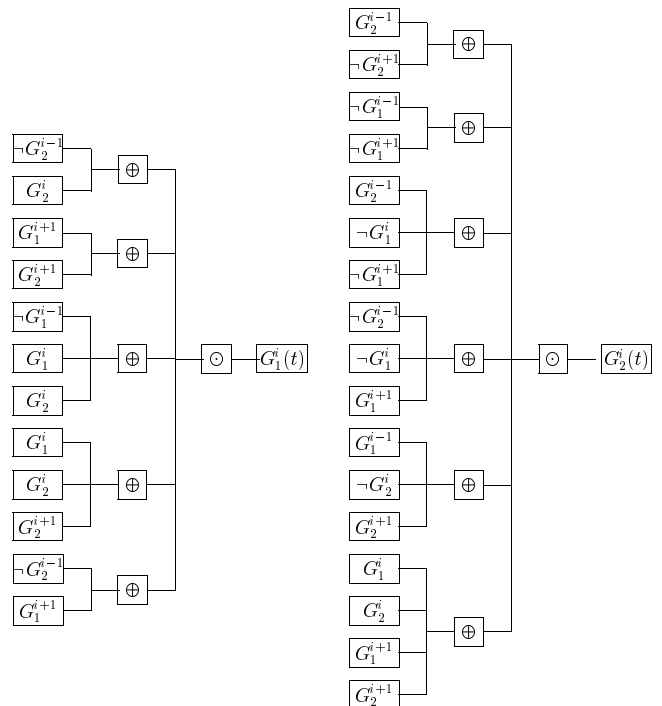


FIG. 5: Boolean representation of the minimal network, minimized conjunctive normal form. G_a^b with $a \in \{1, 2\}$ and $b \in \{i-1, i, i+1\}$ denotes gene a in cell number b . The inputs in the left branches of the trees are given by the genes' states at time $t-1$. \neg denotes NOT, \odot denotes logical AND and \oplus logical OR.

involve a higher number of logical sub-processing steps, i.e. a higher number of genes, hence we will not discuss them here.

Considering the huge number of possible input configurations which the outputs theoretically could depend on, the complexity of the resulting network is surprisingly low. As shown in Fig. 5, the output state of gene G_1 only depends on five different input configurations of at maximum four different inputs, gene number two on six different input configurations of at maximum four different inputs. This indicates that the spatial information flowing into that network is strongly reduced by internal information processing (only a small number of input states leads to output "1"), as expected for the simple stationary target pattern. Nevertheless, this information processing is sufficient to solve the non-trivial task of domain size scaling.

2. Threshold network implementation

Alternatively, the Boolean representation of the pattern formation system can be translated into a three-layered threshold network (Fig. 6). The states of the genes G_1 and G_2 at time t in a cell i and its two neighbor cells $i-1$ and $i+1$ serve as inputs of 11 information-processing genes ("hidden" layer). The state of these

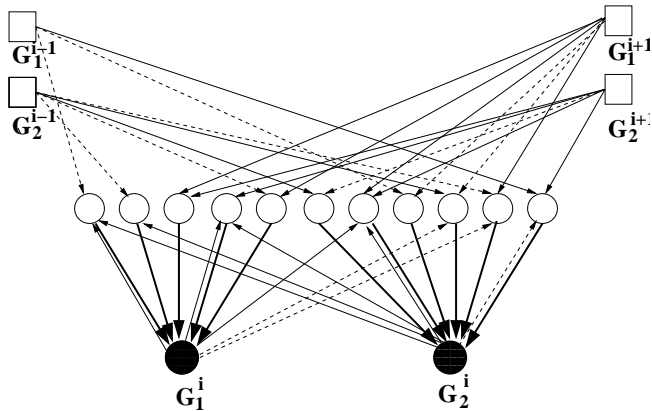


FIG. 6: Threshold network realization of the pattern formation system. Solid line arrows denote links with $w_{ij} = +1$, dashed arrows denote links with $w_{ij} = -1$. The inputs from the genes in the neighbor cells ($G_1^{i-1}, G_2^{i-1}, G_1^{i+1}$ and G_2^{i+1}) are processed by a layer of “hidden genes” (hollow circles) with different thresholds h (as these “genes” perform a logical OR operation, one has $h = k_{in} - 2$). The threshold of gene G_1 is $h_1 = -5$, for gene G_2 one has $h_2 = -6$ (logical AND).

genes then defines the state of G_1 and G_2 in cell i at time $t + 2$ (output layer). Additionally, there is some feedback from G_1 and G_2 to the information processing layer, as expected for the dependence on cell-internal dynamics already present in the cellular automata implementation of the model. The resulting stationary spatial patterns of gene G_1 (the “domain gene”), G_2 (active only at the domain boundary) and the “hidden” genes after system relaxation are shown in Table 2, for a system size of $N_C = 30$ cells. From this seemingly redundant pattern in equilibrium one hardly guesses the higher level of genetic information processing during the self-organizing phase. The network we construct here, regarded as a “developmental module” defining the head-foot polarity through spatially asymmetric gene expression, has a size similar to biological modules (compare, for example, the segment polarity network in *Drosophila* [29]) as well as similar complexity (average connectivity $\bar{K} \approx 3$).

IV. DYNAMICS UNDER NOISE AND CELL FLOW

In the following we will study dynamics and robustness of the model with respect to noise. Two kinds of perturbations frequently occur: Stochastic update errors and external forces caused by a directed *cell flow* due to cell proliferations. Both types of perturbations are very common during animal development, e.g., in *Hydra* cells continuously move from the central body region along the body axis towards the top and bottom, and differentiate into the respective cell types along the way according to their position on the head-foot axis.

Let us define stochastic update errors with probability

gene number	spatial pattern
1	11111111111111111111111111111111
2	11111111111011111111111111111111
3	11111111110000000000000000000000
4	11111111111000000000000000000000
5	11111111111011111111111111111111
6	11111111110111111111111111111111
7	11111111111000000000000000000000
8	10000000011111111111111111111111
9	00000000011111111111111111111111
10	11111111111111111111111111111111
11	11111111111111111111111111111111
G_1	11111111110000000000000000000000
G_2	00000000001000000000000000000000

TABLE II: Spatial gene activity patterns of the network shown in Fig. 6. (stationary patterns after the system has reached equilibrium), $N_C = 30$. The numbers identify the “hidden” genes in Fig. 6 from the left hand side to the right. States were transformed by $\sigma \rightarrow (\sigma + 1)/2$.

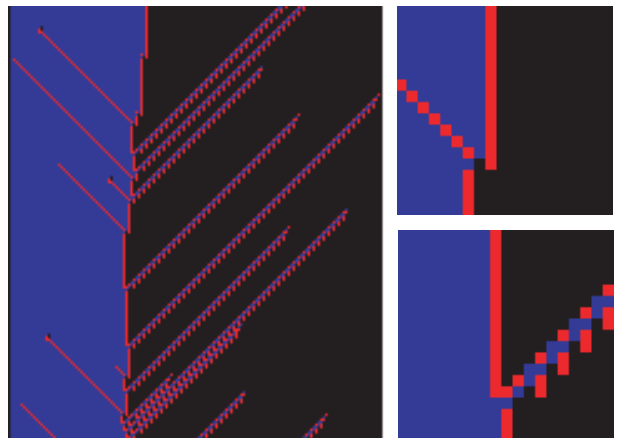


FIG. 7: Quasi-particles, started by stochastic update errors, lead to control of the boundary position under noise (left panel). The Γ particle (top right) leads to readjustment of the boundary two cells to the left, the Δ particle (bottom right) leads to readjustment of the boundary one cell to the right.

p per cell, leading to an average error rate $r_e = p N_C$. Interestingly, this stochastic noise starts moving “particle” excitations in the cellular automaton which, as a result indeed stabilize the developmental structure of the system. To prepare for the details of these effects, define first how we measure the boundary position properly in the presence of noise. Let us use a statistical method to measure the boundary position in order to get conclusive results also for high p : Starting at $i = 0$, we put a “measuring frame” of size w over cell i and the next $w - 1$ cells, move this frame to the right and, for each i , measure the fraction z of cells with state $\sigma = 2$ within the frame. The algorithm stops when z drops below $1/2$ and the boundary position is defined to be $i + w/2$.

It is easy to see that, for not too high p , there are

only two different quasi-particles (i.e. state perturbations moving through the homogeneous phases), as shown in Fig. 7. In the following, these particles are called Γ and Δ . The Γ particle is started in the σ_2 phase by a stochastic error $\sigma_i = 2 \rightarrow \sigma_i \neq 2$ at some $i < \alpha N_C$, moves to the right and, when reaching the domain boundary, readjusts it two cells to the left of its original position. The Δ particle is started in the σ_0 phase by a stochastic error $\sigma_i = 0 \rightarrow \sigma_i \neq 0$ at some $i > \alpha N_C$ and moves to the left. Interaction with the domain boundary readjusts it one cell to the right. Thus we find that the average position α^* of the boundary is given by the rate equation

$$2\alpha^* r_e = (1 - \alpha^*) r_e, \quad (9)$$

i.e. $\alpha^* = 1/3$. Interestingly, for not too high error rates r_e , α^* is independent from r_e and thus from p . If we consider the average boundary position α^* as a system-specific *order parameter* which is controlled by the two quasi-particles, then comparing the solution of Eqn. (9) to the equilibrium position in the noiseless case indicates that the system undergoes a first order phase transition with respect to α^* at $p = r_e = 0$.

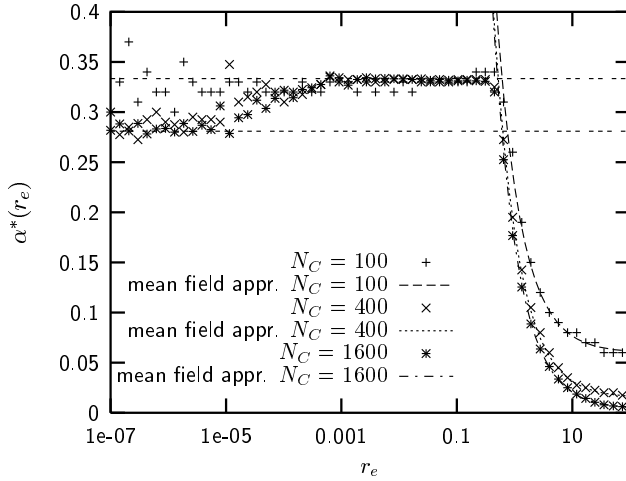


FIG. 8: Average boundary position α^* as a function of the error rate r_e for system sizes $N_C = 100$, $N_C = 400$, and $N_C = 1600$. The abscissa is logarithmic. Numerical data are averaged over 200 different initial conditions with $2 \cdot 10^6$ updates each. The dashed curves show the mean field approximation given by Eqn. (5), the straight dashed lines mark the unperturbed solution $\alpha^* = 0.281$ and the solution under noise, $\alpha^* = 1/3$.

Figs. 9 and 10 show noise dependence and finite size scaling of the transition. In case of a first order phase transition at $r_e = 0$, we would expect a shift of the transition point $r_e^{trans}(s_w)$ towards $r_e = 0$ which is proportional to s_w^{-1} as well as a divergence of the slope at the transition point when s_w is increased, i.e. $d\alpha^*/dr_e(r_e^{trans}) \rightarrow \infty$ when $s_w \rightarrow \infty$.

The shift of $r_e^{trans}(s_w)$ is most easily measured by defining a lower and an upper boundary α_{low}^* and α_{up}^* , respectively (Fig. 9); when α^* crosses these boundaries,

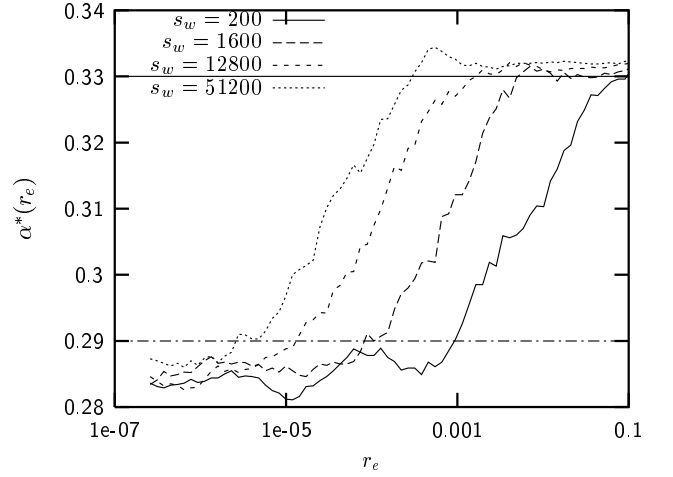


FIG. 9: Average domain boundary position α^* as a function of the error rate r_e , sampled over update windows of different lengths s_w (ensemble statistics, 400 different initial conditions for each data point). The abscissa is logarithmic. With increasing s_w , the transition from the solution $\alpha_{det}^* = 0.281$ under deterministic dynamics to $\alpha^* = 1/3$ under noise is shifted towards $r_e = 0$. The two straight lines define a lower boundary α_{low}^* and an upper boundary α_{up}^* , as explained in the text.

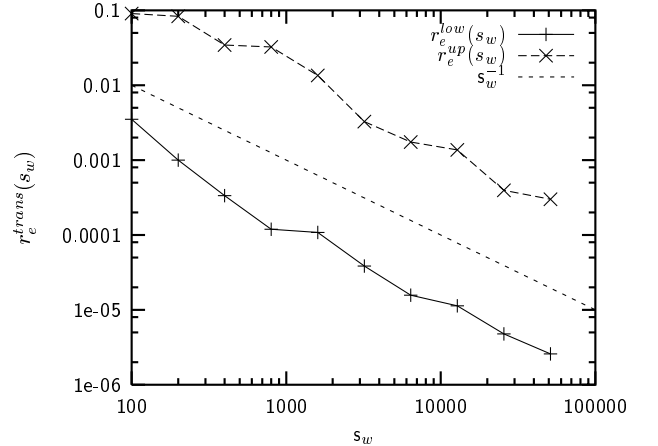


FIG. 10: Finite size scaling of the upper and lower transition points r_e^{up} and r_e^{low} , i.e. the points where α^* crosses α_{low}^* and α_{up}^* , respectively (Fig. 7), as a function of the sampling window length s_w . Both r_e^{up} and r_e^{low} vanish $\propto s_w^{-1}$, as indicated by the line with slope -1 in this log-log-plot.

two transition points r_e^{up} and r_e^{low} are obtained. We find that $r_e^{up} \approx c_{up} s_w^{-1}$ and $r_e^{low} \approx c_{low} s_w^{-1}$ with $c_{up} > c_{low}$ as expected (Fig. 10), which implies that the difference $\Delta r_e^{trans}(s_w) := r_e^{up} - r_e^{low}$ scales as

$$\Delta r_e^{trans}(s_w) = (c_{up} - c_{low}) s_w^{-1}, \quad (10)$$

hence, because $\Delta\alpha^*(r_e^{trans}) = const. = \alpha_{up}^* - \alpha_{low}^*$, indeed $d\alpha^*/dr_e(r_e^{trans})$ diverges when the sampling window size goes to infinity.

The solution $\alpha^* = 1/3$ is stable only for $0 < r_e \leq 1/2$. As shown in Fig. 7, the interaction of a Γ particle with the

boundary needs only one update time step, whereas the boundary readjustment following a Δ particle interaction takes three update time steps. Hence, we conclude that the term on the right hand side of Eqn. (10), which gives the flow rate of Δ particles at the boundary, for large r_e will saturate at $1/3$, leading to

$$2\alpha^* r_e = \frac{1}{3} \quad (11)$$

with the solution

$$\alpha^* = \frac{1}{6} r_e^{-1} + \Theta(N_C) \quad (12)$$

for $r_e > 1/2$. Hence, there is a crossover from the solution $\alpha^* = 1/3$ to another solution vanishing with r_e^{-1} around $r_e = 1/2$. The finite size scaling term $\Theta(N_C)$ can be estimated from the following consideration: for $p \rightarrow 1$, the average domain size created by “pure chance” is given by $\alpha^* = N_C^{-1} \sum_{n=0}^{N_C} (1/3)^n \cdot n \approx (3/4) N_C^{-1}$. If the measuring window has size w , we obtain $\Theta(N_C) \approx (3/4) w N_C^{-1}$. To summarize, we find that the self-organized boundary position is given by

$$\alpha^* = \begin{cases} 0.281 \pm 0.001 & \text{if } r_e = 0 \\ 1/3 & \text{if } 0 < r_e \leq 1/2 \\ (1/6)r_e^{-1} + \Theta(N_C) & \text{if } r_e > 1/2 \end{cases} \quad (13)$$

with a first-order phase transition at $r_e = 0$ and a crossover around $r_e = 1/2$.

Now let us consider the fluctuations of α around α^* given by the master equation

$$\begin{aligned} p^\tau(\alpha) = & 2\alpha r_e p^{\tau-1}(\alpha + 2\delta) + (1 - \alpha) r_e p^{\tau-1}(\alpha - \delta) \\ & + (N_C - r_e) p^{\tau-1}(\alpha) - 2\alpha r_e p^{\tau-1}(\alpha) \\ & - (1 - \alpha) r_e p^{\tau-1}(\alpha) \end{aligned} \quad (14)$$

with $\delta = 1/N_C$. Eqn. (15) determines the probability $p^\tau(\alpha)$ to find the boundary at position α at update time step τ , given its position at time $\tau - 1$. This equation can be simplified as we are interested only in the *stationary probability distribution* of α . It is easy to see that the error rate r_e just provides a time scale for relaxation towards the stationary distribution and has no effect on the stationary distribution itself. Therefore, we may consider the limit $r_e \rightarrow r_e^{max} := N_C$, divide through r_e and neglect the last three terms on the right handside of Eqn. (14) (which become zero in this limit). We obtain

$$p^\tau(\alpha) = 2\alpha p^{\tau-1}(\alpha + 2\delta) + (1 - \alpha) p^{\tau-1}(\alpha - \delta). \quad (15)$$

To study this equation, we consider the continuum limit $N_C \rightarrow \infty$. Let us introduce the scaling variables $x = (\alpha - \alpha^*)\sqrt{N_C}$, $t = \tau/N_C$ and the probability density $f(x, t) = N_C p^\tau(\alpha N_C)$. Inserting these definitions into Eqn. (16) and ignoring all subdominant powers $\mathcal{O}(1/N_C)$, we obtain a Fokker-Planck equation:

$$\frac{\partial f(x, t)}{\partial t} = \left(\frac{\partial^2}{\partial x^2} + 3 \frac{\partial}{\partial x} x \right) f(x, t). \quad (16)$$

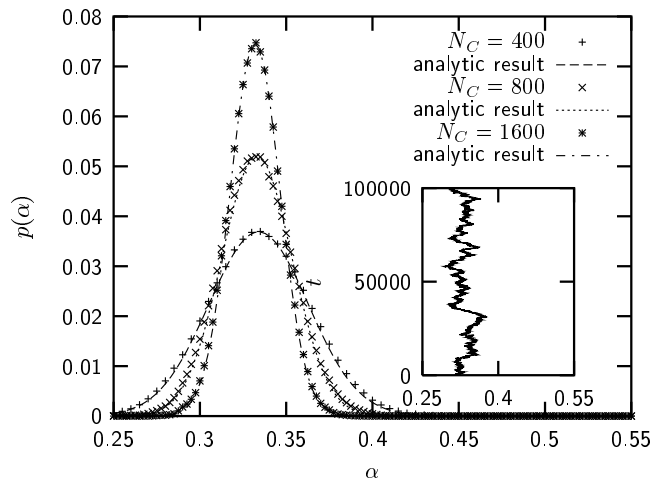


FIG. 11: For the system with stochastic update errors, fluctuations of the boundary position α around the average position $\alpha^* = 1/3$ are Gaussian distributed. The figure compares the numerically obtained stationary probability distribution with the analytic result of Eqn. (18) for three different system sizes. All data are gained for $r_e = 0.1$ and averaged over 100 different initial conditions with $2 \cdot 10^6$ updates each. The inset shows a typical timeseries of the boundary position.

The stationary solution of this equation is given by

$$f(x) = \sqrt{\frac{3}{2\pi}} \exp\left[-\frac{3}{2}x^2\right], \quad (17)$$

i.e. in the long time limit $t \rightarrow \infty$, the probability density for the boundary position α is a Gaussian with mean α^* :

$$p(\alpha, N_C) = \sqrt{\frac{3 N_C}{2\pi}} \exp\left[-\frac{3 N_C}{2} (\alpha - \alpha^*)^2\right]. \quad (18)$$

From Eqn. (18) we see that the variance of α vanishes $\sim 1/N_C$ and the relative boundary position becomes sharp in the limit of large system sizes. Fig. 11 shows that this continuum approximation for $N_C \geq 400$ provides very good correspondence with the numerically obtained probability distributions.

The stochastic nature of boundary stabilization under noise is also reflected by the probability distribution of *waiting times* t for boundary readjustments due to particle interactions: the particle production is a Poisson process with the parameter $\lambda = r_e$ and the waiting time distribution is given by

$$p_{wait}(t) = r_e \exp(-r_e t) \quad (19)$$

with an average waiting time $\langle t \rangle = r_e^{-2}$. Fig. 12 shows the waiting time distributions for different error rates r_e .

In a biological organism, a pattern has to be robust not only with respect to dynamical noise, but also with respect, e.g., to “mechanical” perturbations. In *Hydra*, e.g., there is a steady flow of cells directed towards the animal’s head and foot, due to continued proliferation of

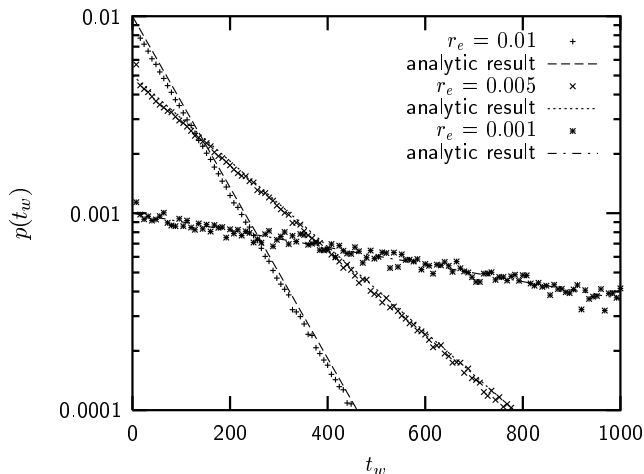


FIG. 12: Probability distribution $p(t)$ of waiting times for boundary readjustments in the model with stochastic update errors for three different values of r_e , semi-log plot. As expected for a Poisson process, $p(t)$ is an exponential.

stem cells [30]; the stationary pattern of gene activity is maintained in spite of this cell flow. Let us now study the robustness of the model with respect to this type of perturbation. Let us consider a constant cell flow with rate r_f , which is directed towards the left or the right system boundary. In Eqn. (9), we now get an additional drift term r_f on the left hand side:

$$2\alpha^* r_e \pm r_f = r_e(1 - \alpha^*), \quad (20)$$

with the solution

$$\alpha^* = \begin{cases} \frac{1}{3} \left(1 - \frac{r_f}{r_e}\right) & \text{if } r_e \geq r_f \\ 0 & \text{if } r_e < r_f \end{cases} \quad (21)$$

for the case of cell flow directed towards the left system boundary (plus sign in eqn. (20)). One observes that α^* undergoes a second order phase transition at the critical value $r_e^{crit} = r_f$. Below r_e^{crit} , the domain size α^* vanishes, and above r_e^{crit} it grows until it reaches the value $\alpha_{max}^* = 1/3$ of the system without cell flow. For cell flow directed towards the right system boundary (minus sign in eqn. (20)), we obtain

$$\alpha^* = \begin{cases} \frac{1}{3} \left(1 + \frac{r_f}{r_e}\right) & \text{if } r_f \leq 2r_e \\ 1 & \text{if } r_f > 2r_e. \end{cases} \quad (22)$$

In this case, the critical cell flow rate is given by $r_f = 2r_e$, for cell flow rates larger than this value the σ_2 -domain extends over the whole system, i.e. $\alpha^* = 1$. Fig. 13 compares the results of numerical simulations with the mean field approximation of Eqn. (20). In numerical simulations, cell flow is realized by application of the translation operator $\Theta \sigma_i := \sigma_{i+1}$ to all cells with $0 \leq i < N_C - 1$ every r_f^{-1} time steps and leaving σ_{N_C-1} unchanged. In case of cell flow directed to the right system boundary, in the

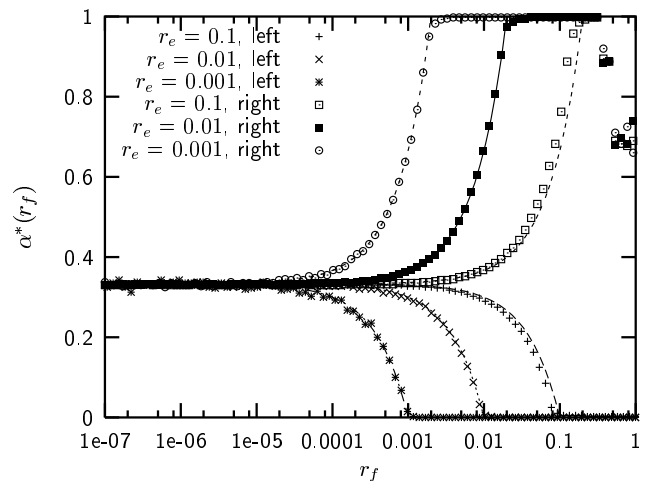


FIG. 13: Average domain size α^* as a function of the the cell flow rate r_f for three different error rates r_e ; numerical data (crosses and points) were sampled over 10 different initial conditions and $1e6$ updates for each data point. “Left” indicates cell flow directed to the left system boundary, “right” to the right system boundary, respectively. The dashed lines are the corresponding solutions of Eqn. (20).

limit $r_f \rightarrow 1$ the boundary position α^* detected in numerical simulations deviates from the mean field prediction, due to a boundary effect at the left system boundary (stochastic production of finite lifetime stationary oscillators, leading to intermittent flows of Γ particles through the system).

To summarize this part, we see that in the model stochastic errors in dynamical updates for $r_e > r_f$ indeed *stabilize* the global pattern against the mechanical stress of directed cell flow.

V. SUMMARY AND DISCUSSION

In this paper we considered the dynamics of pattern formation motivated by animal morphogenesis and the largely observed participation of complex gene regulation networks in their coordination and control. We therefore chose a simple developmental problem to study toy models of interacting networks that control pattern formation and morphogenesis in this setting. In particular, the goal was to explore how networks can offer additional mechanisms beyond the standard diffusion based process of the Turing instability. Our results suggest that main functions of morphogenesis can be performed by dynamical networks without relying on diffusive biochemical signals, but using local signaling between neighboring cells. This includes solving the problem of generating global position information from purely local interactions. But also it goes beyond diffusion based models as it offers solutions to developmental problems that are difficult for such models and avoids their inherent problem of fine tuned model parameters. It may be not too far fetched

to speculate that some developmental processes as, e.g., the establishment of position information, may rely on this type of internal information processing rather than on interpretation of, e.g., chemical gradients. As only ingredient to the present model, symmetry has to be broken locally by a spatially asymmetric receptor distribution, e.g., as proposed in [19], to provide the necessary input information. Also hybrid approaches are conceivable. For example such broken symmetry could be provided by a gradient, even without fine-tuning (contrary to standard gradient-based models) since only the direction of the gradient has to be read out.

The network model derived here performs accurate regulation of position information and robust *de novo* pattern formation from random conditions, with a mechanism based on local information transfer rather than the Turing instability. Non-local information is transmitted through soliton-like quasi-particles instead of long-range gradients. Two realizations as discrete dynamical networks, Boolean networks and threshold networks, have been developed. The resulting networks have size and complexity comparable to developmental gene regulation modules as observed in animals, e.g., *Drosophila* [29] or *Hydra* [6]. The threshold networks (as models for transcriptional regulation networks) process position information in a hierarchical manner; in the present study, hierarchy levels were limited to three, but realizations with more levels of hierarchy, i.e. more “pre-processing” of information are also possible. Similar hierarchical and modular organization are typical signatures of gene regulatory networks in organisms [18].

Robustness of the model is studied in detail for two types of perturbations, stochastic update errors (noise) and directed cell flow. A first order phase transition is observed for vanishing noise and a second order phase transition at increasing cell flow. Fluctuations of the noise-controlled boundary position were studied numerically for finite size systems and analytically in the continuum limit. We find that the relative size of fluctuations vanishes with $1/N_C$, which means that the boundary position becomes sharp in the limit of large system sizes. Dynamics under cell flow is studied in detail numerically and analytically by a mean field approximation. A basic observation is that noise-induced perturbations act as quasi-particles that stabilize the pattern against the directed force of cell flow. At a critical cell flow rate, there is a second order phase transition towards a vanishing domain size or a domain extending over the whole system, depending on the direction of cell flow, respectively.

Several extensions of this model are conceivable. In the present model, the cell flow rate r_f is considered as a free parameter, the global pattern, however, can be controlled easily by an appropriate choice of the error rate r_e . This may suggest to extend the model by introduction of some kind of dynamical coupling between r_e and r_f , treating r_f as a function of r_e . Interestingly, similar approaches have been studied by Hogeweg [31] and Furusawa and Kaneko [32, 33]: In both models of

morphogenesis, the rate of cell divisions is controlled by cell differentiation and cell-to-cell signaling. Dynamics in both models, however, is deterministic. An extension of our model as outlined above may open up for interesting studies how *stochastic* signaling events could control and stabilize a global expression pattern and cell flow as an integrated system. Other possible extensions of the model concern the dimensionality: In two or three dimensions other mechanisms of symmetry breaking might be present, possibly leading to new, interesting dynamical effects.

A Java applet simulation of the model can be found at [34].

VI. ACKNOWLEDGEMENTS

We thank T.C.G. Bosch, T.W. Holstein, and U. Technau for pointing us to current questions in Hydra development. T.R. acknowledges financial support from the Studienstiftung des deutschen Volkes (German National Merit Foundation).

APPENDIX A: GENETIC ALGORITHM SEARCHES

Let us briefly recapitulate here how the rule table of the model has been obtained by the aid of a genetic algorithm.

1. Definition of the GA

In order to find a set \mathcal{F} of update rules that solve the problem as formulated in section II, cellular automata have been evolved using genetic algorithms [35]. Genetic algorithms are population-based search algorithms, which are inspired by the interplay of random mutations and selection as observed in biological evolution [36]. Starting from a randomly generated population of P rule tables f_n , the algorithm optimizes possible solutions by evaluating the fitness function

$$\Phi(f_n) = \frac{1}{(T_u - T) \cdot N_C} \sum_{t=T_u-T}^{T_u} \left(\sum_{i=0}^{[\alpha \cdot N_C]-1} \delta_{\sigma_i^n(t),2} + \sum_{i=[\alpha \cdot N_C]}^{N_C-1} \{1 - \delta_{\sigma_i^n(t),2}\} \right). \quad (\text{A1})$$

The optimization algorithm then is defined as follows:

1. Generate a random initial population $\mathcal{F} = \{f_1, \dots, f_P\}$ of rule tables.
2. Randomly assign system sizes $N_C^{\min} \leq N_c^n \leq N_C^{\max}$ to all rule tables.

3. For each rule table, generate a random initial state vector.
4. Randomly mutate one entry of each rule table (generating a population \mathcal{F}^* of mutants).
5. Iterate dynamics over T_u time steps for \mathcal{F} and \mathcal{F}^* .
6. Evaluate $\Phi(f_n)$ and $\Phi(f_n^*)$ for all rule tables $0 < n \leq P$, averaging over the past $T_u - T$ update steps (with an additional penalty term if f_n does not converge to a fixed point).
7. For each n , replace f_n with f_n^* , if $\Phi(f_n) \leq \Phi(f_n^*)$.
8. Replace the least fit solution by a duplicate of the fittest one.
9. Go back to step 2 and iterate.

The outcome of this search algorithm is a set of rule tables, which then can be “translated” into (spatially coupled) Boolean networks or threshold networks with suitable thresholds. This yields a set of (minimal) dynamical networks which solve the pattern formation task by means of internal information processing.

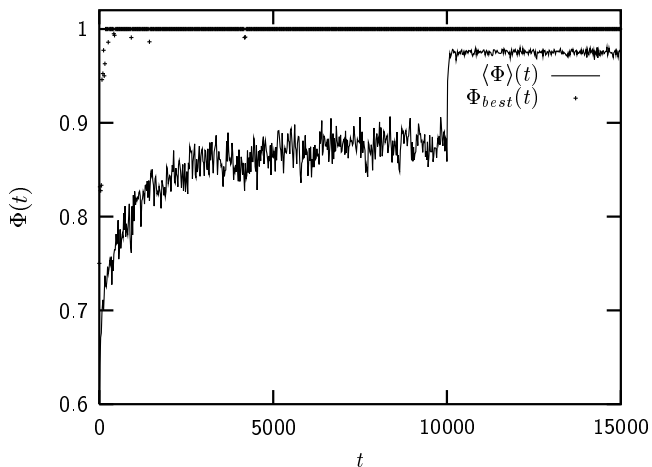


FIG. 14: Average fitness $\langle \Phi \rangle(t)$ of the mutant population \mathcal{F}^* and fitness of the highest fitness mutant $\Phi_{best}(t)$ as a function of simulation time during the genetic algorithm run that lead to the high fitness solution used in this paper. At time step 10000 mutations were turned off, in order to test the established population of optimized rule tables under different initial conditions (this corresponds to the sharp increase of $\langle \Phi \rangle(t)$ at time step 10000). The evolved population of rule tables has an average fitness of about 0.98, independent from the initial conditions and system size N_C (in the tested range, i.e. $15 \leq N_C \leq 150$).

2. Evolution of cellular automata

The genetic algorithm sketched above is run with the following parameter choices: $15 \leq N_C \leq 150$, i.e. during

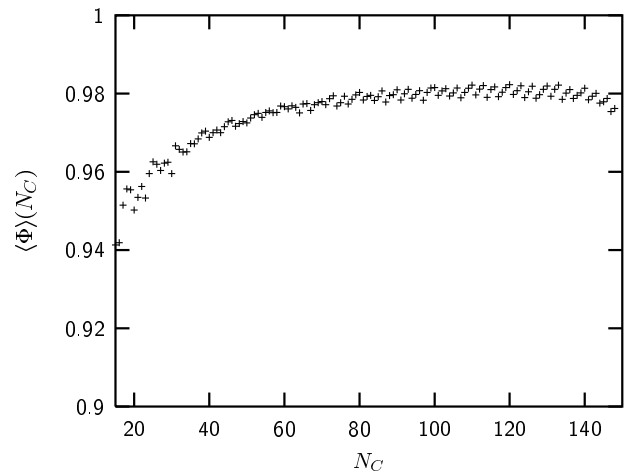


FIG. 15: Average fitness of the highest fitness rule table as a function of the system size N_C . For system sizes $N_C \geq 80$ the fitness is almost constant at about 0.98. Notice that the decrease of the fitness for small N_C is an effect of the dynamics, not of the genetic algorithm implementation (all N_C in the range $15 \leq N_C \leq 150$ were tested with equal probability), hence the dynamics of pattern formation may impose a lower boundary on the range of system (animal) sizes tolerated by natural selection.

GA runs the system size is varied randomly between 15 and 150 cells, and the population size is set to $P = 100$. Fig. 14 shows the fitness of the highest fitness mutant and the average fitness of the population as a function of successive mutation steps during optimization. A useful solution is found rather quickly (after about 200 updates), with further optimization observed during further 10000 generations. At time step 10000 mutations are turned off, thus now the average fitness of the established population under random initial conditions and random fluctuations of the system size N_C is tested. The average fitness $\Phi \approx 0.98$ indicates a surprisingly high robustness against fluctuations in the initial start pattern, indicating that the system is capable of *de novo pattern formation*. In the “fitness picture”, Fig. 15 confirms that the dynamically regulated domain size ratio $\alpha/(1 - \alpha)$ indeed is independent of system size (proportion regulation), there is only a weak decay of the fitness at small values of N_C . Interestingly, one also observes that for regeneration of Hydra polyps from random cell aggregates a minimum number of cells is required [1]. The model suggests that this observation might be explained by the dynamics of an underlying pattern generating mechanism, i.e. that there has to be a minimum diversity in the initial condition for successful *de novo* pattern formation.

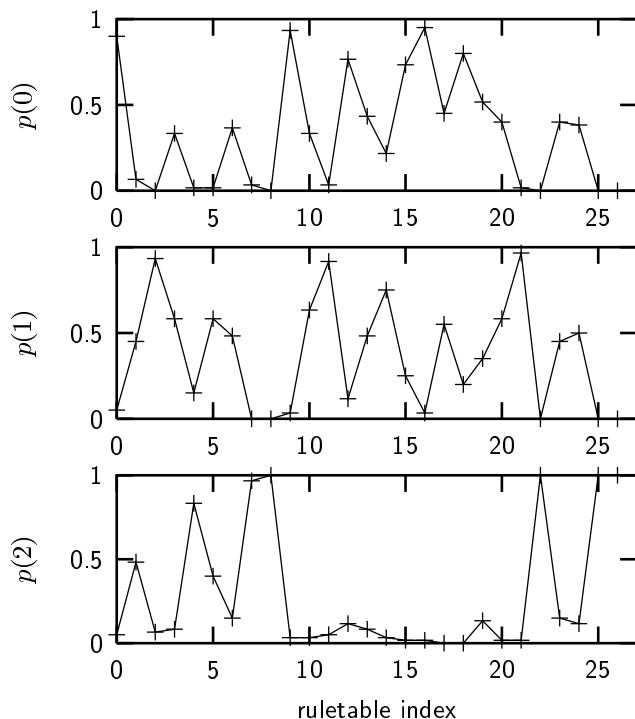


FIG. 16: Frequency distribution $p(\sigma_i)$ of outputs as a function of the rule table index as denoted in table 1. Ensemble statistics is taken over 80 different solutions with $\Phi \geq 0.96$. The upper panel shows the distribution for $\sigma_i = 0$, the middle panel the distribution for $\sigma_i = 1$ and the lower panel the distribution for $\sigma_i = 2$.

APPENDIX B: STATISTICAL ANALYSIS OF SOLUTIONS

An interesting question is how “difficult” it would be for an evolutionary process driven by random mutations and selection to find solutions for the pattern formation problem based on neighbor interactions between cells. As we showed above, the genetic algorithm finds the correct solution fast, however, this does not necessarily mean that biological evolution could access the same solution as fast. If there is only one, singular solution, evolution may never succeed finding it, as the genotype which already exists cannot be modified in an arbitrary way without possibly destroying function of the organism (*developmental constrains*). To illustrate this point, we generated an ensemble of $N_E = 80$ different solutions with $\Phi \geq 0.96$ and performed a statistical analysis of the rule table structure.

As one can see in Fig. 16, some positions in the rule table are quite fixed, i.e., there is not much variety in the outputs, whereas other positions are more variable. However, the output frequency distribution alone does not allow to really judge the “evolvability” of the solutions: if there are strong correlations between most of the rule table entries, evolutionary transitions from one solution to another would be almost impossible. To check



this point, we studied statistical two point correlations between the rule table entries. The probability for finding state σ at position a and state σ' at rule table position b is given by

$$p^{ab}(\sigma, \sigma') = \frac{1}{N_E} \sum_{n=1}^{N_E} \delta_{\sigma^n(a), \sigma} \cdot \delta_{\sigma^n(b), \sigma'}, \quad (\text{B1})$$

where δ is the Kronecker symbol and n runs over the statistical ensemble of size N_E . The two point correlation between a and b then is defined as

$$C^{ab} = c_1 \left(\max_{(\sigma, \sigma')} p^{ab}(\sigma, \sigma') - c_2 \right) \quad (\text{B2})$$

with $c_1 = 9/8$ and $c_2 = 1/9$ to obtain a proper normalization with respect to the two limiting cases of equal probabilities ($p^{ab}(\sigma, \sigma') = 1/9 \quad \forall(\sigma, \sigma')$) and $p^{ab}(\sigma, \sigma') = 1$ for $\sigma = \tilde{\sigma}$, $\sigma' = \tilde{\sigma}'$ and $p^{ab}(\sigma, \sigma') = 0$ for all other (σ, σ') . Fig. 17 shows the frequency distribution of $C^{ab}(\sigma, \sigma')$, averaged over all possible pairs (a, b) . About 65% of rule table positions are strongly correlated ($C^{ab} = 1.0$), the rest shows correlation values between 0.3 and 1.0. Hence, we find that the space of solutions is restricted, nevertheless there is variability in several rule table positions. To summarize this aspect, the pattern formation mechanism studied in this paper shows considerable robustness against rule mutations, however, a “core module” of rules is always fixed. Interestingly, a similar phenomenon is observed in developmental biology: Regulatory “modules” involved in developmental processes often are evolutionarily very conservative, i.e., they are shared by almost all animal phyla [18], while morphological variety is created by (few) taxon specific genes [6] and “rewiring” of existing developmental modules.

-
- [1] U. Technau et al., *Proc. Natl. Acad. Sci. (USA)*, **97**, 12127 (2000).
- [2] T.C.G. Bosch, *Comp. Biochem. and Physiol. B*, **136**, 185 (2003).
- [3] A.M. Turing, *Phil. Trans. Roy. Soc. B*, **237**, 37 (1952).
- [4] A. Gierer and H. Meinhardt, *Kybernetik* **12**, 30 (1972).
- [5] H. Meinhardt and A. Gierer, *BioEssays* **22.8**, 753 (2000).
- [6] T.C.G. Bosch and K. Khalturin, *Canadian Journal of Zoology* **80**, 1670-1677 (2002).
- [7] E.R. Jackson, D. Johnson and W.G. Nash, *J. Theor. Biol.* **119**, 379 (1986).
- [8] S.A. Kauffman, *J. Theor. Biol.* **22**, 437 (1969).
- [9] S.A. Kauffman, *The Origins of Order: Self-Organization and Selection in Evolution*, Oxford University Press, New York, 1993.
- [10] J. Slack, *Mech. Devel.* **41**, 257, 9100-9107 (1997).
- [11] I. Salazar-Ciudad, J. Garcia-Fernandez and R.V. Sole, *J. Theor. Biol.* **205**, (2000).
- [12] R.V. Sole, I. Salazar-Ciudad and J. Garcia-Fernandez, *Physica A* **305**, 640 (2002).
- [13] T. Rohlf and S. Bornholdt, submitted (2003); cond-mat/0312366.
- [14] S. Wolfram, *Rev. Mod. Phys.*, **55**, 601 (1983); *Physica D*, **10**, 1 (1984); *Nature (London)*, **311**, 419 (1984).
- [15] S. Thomsen, A. Till, C. Beetz, J. Wittlieb, K. Khalturin, and T.C.G. Bosch, *Mech. Devel.*, in press (2003).
- [16] L. Wolpert, *J. Theor. Biol.*, **25**, 37 (1952).
- [17] W.A. Müller, Pattern control in Hydra: basic experiments and concepts. In: *Experimental and Theoretical Advances in Biological Pattern Formation*, eds. H.G. Othmer, P.K. Maini, and J.D. Murray, Plenum Press, New York (1993).
- [18] E.H. Davidson, *Genomic Regulatory Systems. Development and Evolution*. Academic Press (2001).
- [19] A. Marciniac-Czochra, *J. Biol. Syst.* **11**, 293 (2003).
- [20] K.E. Kürten, *Phys. Lett. A* **129(3)**, 157 (1988).
- [21] K.E. Kürten, *J. Phys. A* **1 21**, L615-L619 (1988).
- [22] A. Wagner, *Proc. Natl. Acad. Sci. USA* **91**, 4387-4391 (1994).
- [23] S. Bornholdt and K. Sneppen, *Proc. R. Soc. Lond. B* **267**, 2281-2286 (2000).
- [24] S. Bornholdt and T. Rohlf, *Phys. Rev. Lett.* **84**, 6114 (2000).
- [25] T. Rohlf and S. Bornholdt, *Physica A* **310**, 245 (2002).
- [26] T. Rohlf and S. Bornholdt, *Gene regulatory networks: A discrete model of dynamics and topological evolution*, In: *Function and regulation of cellular systems: experiments and models*, eds. A. Deutsch, J. Howard, M. Falcke and W. Zimmermann, 233-239, Birkhäuser, Basel (2004).
- [27] J.P. Crutchfield and M. Mitchell, *Proc. Natl. Acad. Sci. (USA)*, **92**, 10742 (1995).
- [28] E.J. McCluskey, *Bell Syst. Techn. J.*, **35**, 1417-1444 (1956).
- [29] G. von Dassow, E. Meir, E.M. Munro and G.M. Odell, *Nature* **406**, 188-192 (2000).
- [30] C. N. David and R. D. Campbell, *J. Cell. Sci.* **11**, 557 (1972).
- [31] P. Hogeweg, *J. Theor. Biol.* **203**, 317-333 (2000).
- [32] C. Furusawa and K. Kaneko, *Phys. Rev. Lett.* **84**, 6130 (2000).
- [33] C. Furusawa and K. Kaneko, *J. Theor. Biol.* **224**, 413-435 (2003).
- [34] <http://www.theo-physik.uni-kiel.de/~rohlf/development.html>
- [35] M. Mitchell, P. Hraber and J.P. Crutchfield, *Physica D* 361-391 (1994).
- [36] J.H. Holland, *Adaptation in natural and artificial systems*. University of Michigan Press, Ann Arbor (1975).